ACS Photonics

pubs.acs.org/journal/apchd5

Article

Tunable Thermal Emission of Subwavelength Silica Ribbons

Juan José García-Esteban, Jorge Bravo-Abad, and Juan Carlos Cuevas*

Cite This: *ACS Photonics* 2022, 9, 3679–3684

Read Online

ACCESS | Metrics & More | Article Recommendations | Supporting Information

ABSTRACT: The thermal properties of individual subwavelength objects, which defy Planck's law, are attracting significant fundamental and applied interest in different research areas. Special attention has been devoted to anisotropic structures made of polar dielectrics featuring thicknesses smaller than both the thermal wavelength and the skin depth. Recently, a novel experimental technique has enabled the measurement of the thermal emissivity of anisotropic SiO_2 nanoribbons (with thicknesses on the order of 100 nm), demonstrating that their emission properties can be largely tuned by adjusting their dimensions. However, despite the great interest aroused by these results, their rigorous theoretical analysis has remained elusive due to the computational challenges arising from the vast difference in the length scales involved in the problem. In this work, we present a systematic theoretical analysis of the thermal emission properties of these dielectric nanoribbons based on simulations within the framework of fluctuational electrodynamics carried out with the boundary element method implemented in the SCUFF-EM code. In agreement with the experiments, we show that the emissivity of these subwavelength structures can be largely tuned and enhanced over the thin-film limit. We elucidate that the peculiar emissivity of these nanoribbons is due to the very anisotropic thermal emission that originates from the phonon polaritons of this material and the properties of the waveguide modes sustained by these dielectric structures. Our work illustrates the rich thermal properties of subwavelength objects, as well as the need for rigorous theoretical methods that are able to unveil the complex thermal emission phenomena emerging in this class of systems.

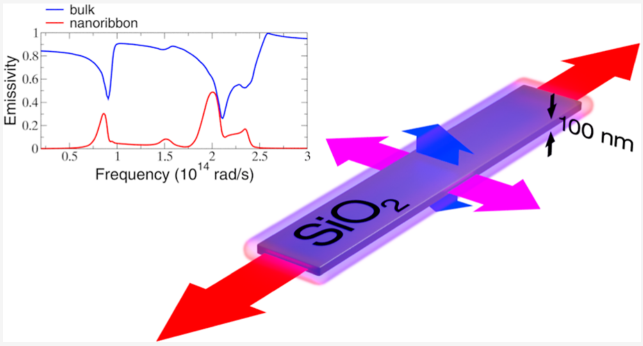

KEYWORDS: *thermal emission, subwavelength objects, silica nanoribbons, anisotropic*

■ INTRODUCTION

Controlling the thermal emission of finite-sized objects is important for applications such as passive radiative cooling[1−7] or thermal extraction.[8,9] From a more fundamental point of view, our understanding of thermal radiation phenomena has been traditionally based on Planck's law and the concept of blackbody.[10] This law sets an upper limit, known as the blackbody or Planckian limit, for the amount of energy that an object can emit in the form of electromagnetic waves. Moreover, according to Planck's law, the thermal emission of an object is incoherent, of broad band, almost isotropic, and unpolarized. However, this common wisdom has been challenged in recent years in the context of nanophotonics.[11] Since Planck's law is based on ray optics, the description of the thermal emission of objects with dimensions smaller than the thermal wavelength λ_{Th} given by Wien's law (~10 μm at room temperature) is out of its scope.[12,13] Such subwavelength objects may exhibit very special thermal emission properties. Thus, it has been predicted that under special circumstances they can even overcome the blackbody limit,[14,15] which in turn can lead to the phenomenon of far-field super-Planckian radiative heat transfer.[15,16] Let us clarify that the blackbody limit can be overcome in the far field because the emission of an object is in fact determined by its absorption cross section, which can be larger than the geometrical cross section used in Planck's law to compute the thermal emission.

The failure of Planck's law to describe the thermal emission of subwavelength objects has been reported, for instance, in experiments on the thermalization of an optical fiber thinner than λ_{Th}.[17] In recent years, there has been a renewed effort to develop experimental techniques to measure the thermal emission properties of individual subwavelength objects, with special attention devoted to dielectric structures such as individual antennas.[18−23] On the theoretical front, the description of these properties continues to be a challenge. There exists a rigorous theoretical framework known as fluctuational electrodynamics,[24] and different numerical methods have already been developed in this framework to describe the thermal radiation properties of objects of arbitrary

Received: July 29, 2022
Published: October 26, 2022

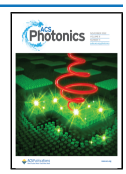

https://doi.org/10.1021/acsphotonics.2c01183
ACS Photonics 2022, 9, 3679−3684

size and shape.[25−32] However, such a description typically requires solving Maxwell's equations in complex geometries and involving very different dimensions, such that they are often out of scope of those methods.

In this context, Shin and coworkers reported in 2019 the development of a novel experimental platform to measure the thermal emissivity of an individual nanoscale object.[20] This platform makes use of very sensitive thermometry to measure the thermal conductance of an object in combination with optical modeling to extract its thermal emissivity. This technique was used to investigate the thermal emission of anisotropic nanoribbons made of a polar dielectric (SiO_2) with a thickness of 100 nm, much smaller than both λ_{Th} and the skin depth of the material. Interestingly, these authors showed that the total emissivity of these nanoribbons can be tuned by adjusting their lateral dimensions and found that they can exhibit over 8.5-fold enhancement in the emissivity compared with the thin-film limit. This behavior was attributed to the contribution of surface phonon polaritons. However, no actual calculations/simulations for the emissivity of these silica nanoribbons have been reported thus far, which is mainly due to the computational challenges arising from the fact that some of their dimensions are of the order of or bigger than 100 μm.

The goal of this work is to fill this theoretical gap and to provide a systematic study of the thermal emission of silica nanoribbons. Using the boundary element method (BEM) implemented in the SCUFF-EM code,[33−35] here we show how the emissivity of these subwavelength ribbons can be tuned by adjusting their dimensions. In agreement with the experimental findings by Shin et al.,[20] we show that the emissivity of these nanoribbons is enhanced with respect to the thin-film limit and that their thermal properties can be traced back to the peculiar properties of electromagnetic modes sustained by these dielectric nanostructures. Overall, our work illustrates the potential that anisotropic subwavelength objects offer for thermal emission tuning.

RESULTS AND DISCUSSION

Motivated by the experimental work of Shin et al.,[20] our goal in this manuscript is to analyze theoretically the thermal emission of anisotropic silica (SiO_2) ribbons, see Figure 1a, whose dimensions will be denoted by L (length), W (width), and τ (thickness). Following Shin et al.,[20] we shall mainly focus on subwavelength ribbons with thicknesses on the order of 100 nm (much smaller than both λ_{Th} at room temperature and the SiO_2 skin depth at any frequency), while the other two dimensions can be much bigger (even bigger than λ_{Th}). In particular, we shall explore ribbon lengths up to 100 μm. We are interested in the total power emitted by these silica ribbons, which is given by[36]

$$P_{em} = \pi A \int_0^\infty d\omega \, I_{BB}(\omega, T) \varepsilon(\omega) \tag{1}$$

where A is the total area of the object, $\varepsilon(\omega)$ is the angular-averaged frequency-dependent emissivity of the body, and $I_{BB}(\omega,T)$ is the frequency-dependent Planck distribution at a temperature T given by

$$I_{BB}(\omega, T) = \frac{\omega^2}{4\pi^3 c^2} \frac{\hbar\omega}{e^{\hbar\omega/k_B T} - 1} \tag{2}$$

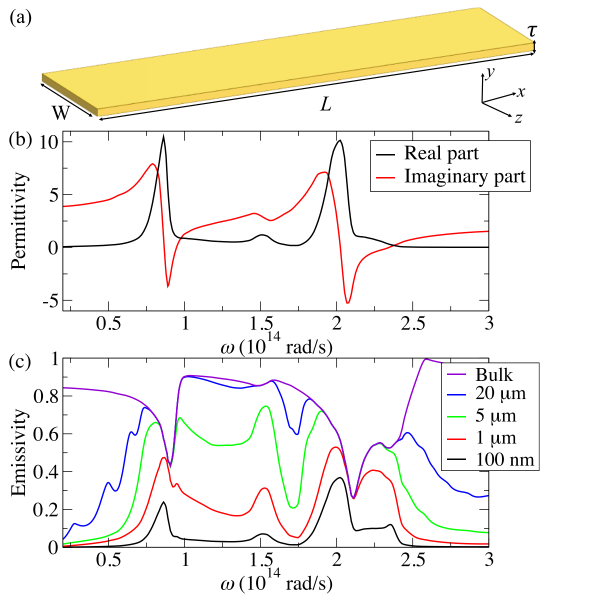

Figure 1. (a) Schematic representation of the silica ribbons considered in this work of length L, width W, and thickness τ. (b) Real and imaginary parts of the electrical permittivity of SiO_2 in the frequency range of interest. (c) Emissivity spectra of silica thin films of different widths, including the case of an infinite surface (bulk).

In the case of a black body, $\varepsilon(\omega) = 1$ for all frequencies and the total emitted power is given by Stefan−Boltzmann law: $P_{em,BB} = A\sigma T^4$, where $\sigma = 5.67 \times 10^{-8}$ W/(m^2K^4). The theoretical challenge lies in this case in the calculation of the emissivity $\varepsilon(\omega)$, which requires the solution of Maxwell equations with thermally fluctuating electrical currents as sources of the electromagnetic radiation, something that is highly non-trivial due to the dimensions of the studied silica ribbons. In this work, the emissivity of these objects was calculated using the code SCUFF-EM, which implements a fluctuating-surface-current approach to the radiative heat transfer problem and provides numerically exact results within the framework of fluctuational electrodynamics.[33−35] In particular, SCUFF-EM makes use of the BEM, a robust and powerful numerical implementation of the surface-integral formulation of classical electromagnetism. To our knowledge, this BEM-based approach is the only method able to deal with finite objects of the size of the nanoribbons investigated in this work (see the Supporting Information for convergence tests of this approach). The input in the calculation of the emissivity, apart from the geometry, is the frequency-dependent permittivity of SiO_2, which was taken from tabulated values.[37] The real and imaginary parts of this permittivity are shown in Figure 1b in the frequency range of interest for our study. Notice the existence of two phonon-polariton resonances, that is, two peaks in the imaginary part of the dielectric function, which are associated with the optical phonon modes in this polar dielectric. Notice also that these resonances are accompanied by regions where the real part of the permittivity becomes negative (the so-called Reststrahlen bands).

As a reference for our forthcoming discussions, we show in Figure 1c the frequency-dependent emissivity of silica films with thicknesses ranging from 100 nm (deep subwavelength) to the bulk situation (corresponding to an infinite surface). In virtue of Kirchhoff's law, these emissivities are equal to the corresponding absorption coefficients, which for infinite films

https://doi.org/10.1021/acsphotonics.2c01183
ACS Photonics 2022, 9, 3679−3684

can be easily calculated with standard methods of classical optics (we used in particular a scattering matrix approach,[38] see Figure S1 in Supporting Information). Another important metric to evaluate the thermal emission of a single object is the total emissivity, which is defined as the ratio between the total power emitted and the corresponding power emitted by a blackbody of the same size and shape: $\varepsilon_{\mathrm{Total}} = P_{\mathrm{em}}/P_{\mathrm{em,BB}}$, which only depends on temperature. This was, in fact, the physical quantity measured by Shin et al.[20] For the silica films of Figure 1c, this total emissivity at room temperature (300 K) ranges from 0.061 for a thickness of 100 nm to 0.79 for the infinite surface.

To establish a detailed comparison with the experimental results reported in the work of Shin et al.,[20] we focus now on the analysis of the emissivity spectra of silica nanoribbons of thickness τ = 100 nm. In Figure 2a we show the emissivity for

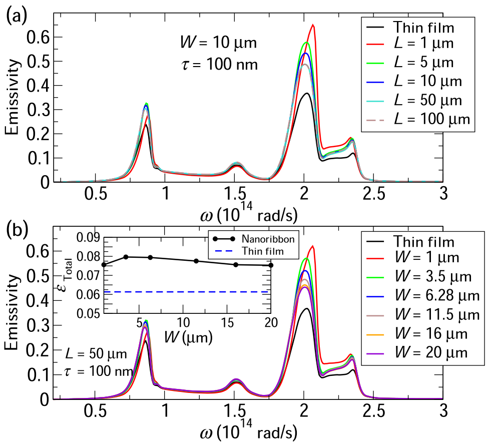

Figure 2. (a) Emissivity as a function of the frequency for SiO_2 nanoribbons of width W = 10 μm and τ = 100 nm and different values of length L. We also include the result for a thin film of τ = 100 nm (black solid line). Notice that, upon increasing the length, the emissivity saturates at $L \sim 50$ μm. (b) Emissivity as a function of the frequency for SiO_2 nanoribbons of length L = 50 μm, thickness τ = 100 nm, and different values of width W. We also include the result for a thin film of τ = 100 nm (black solid line). The inset shows the corresponding total emissivity (integrated over frequencies) at room temperature (300 K) as a function of the ribbon width. The result for a thin film of thickness 100 nm is shown as a blue dashed line for reference.

nanoribbons of width W = 10 μm and varying length (L), and we also include the case of an infinite thin film for comparison. As one can see, the emissivity of the nanoribbons is higher than for the thin film case, and it is mainly dominated by the frequencies around the phonon-polariton resonances. More importantly, as the length of the ribbons increases, the emissivity saturates at $L \sim 50$ μm, which allows us to conclude that we are indeed able to simulate the actual nanoribbons that were experimentally studied.[20] Let us recall that Shin et al. reported results for nanoribbons with a length ranging from 100 to 800 μm. In this regard, we shall fix the length from now on to L = 50 μm, which for all practical purposes corresponds to an infinitely long ribbon.

To clarify the role of the nanoribbons' width, a central issue in the experimental work,[20] we present in Figure 2b the emissivity spectra of ribbons with τ = 100 nm, L = 50 μm, and varying width, ranging from W = 1 μm to W = 20 μm (we also include the result for a thin film for comparison). As it is evident from these results, there is no drastic impact of the ribbon's width in the explored range. This is also apparent in the inset of Figure 2b, where we show the room-temperature total emissivity as a function of ribbon's width. Notice, however, that in all cases, the finite width results in a higher emissivity than the corresponding thin film. Shin et al. investigated nanoribbons of two different widths and obtained total emissivities at 300 K of $\varepsilon_{\mathrm{Total}} = 0.105 \pm 0.025$ for W = 11.5 μm and $\varepsilon_{\mathrm{Total}} = 0.170 \pm 0.030$ for W = 6.28 μm. This has to be compared with our results of $\varepsilon_{\mathrm{Total}}$ = 0.0775 for W = 11.5 μm and $\varepsilon_{\mathrm{Total}}$ = 0.0794 for W = 6.28 μm. Given the large experimental uncertainties and the extreme difficulty of these measurements, the agreement between theory and experiment is satisfactory.

The main conclusion of our analysis so far is that, in agreement with the experimental observations, the emissivity of a silica film can be enhanced by forming ribbons, that is, by reducing its width. What is the reason for this enhancement? In simple terms, it must be due to the contribution to the total emission coming from the lateral facets of the ribbons, which is absent in the film case. To test this idea, we have investigated the directional absorption cross section C_{abs} of these ribbons for different directions and polarizations, which in virtue of Kirchhoff's law coincides with the corresponding directional emissivity. These cross sections were also computed with the SCUFF-EM code (module SCUFF-SCATTER).[35] In Figure 3a we show C_{abs} for a nanoribbon with L = 50 μm, W = 10 μm,

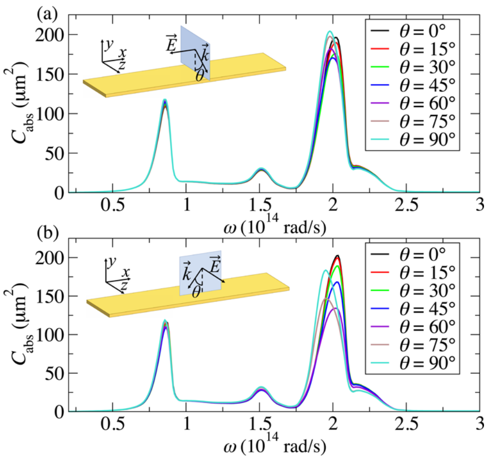

Figure 3. (a) Absorption cross section as a function of the frequency for a SiO_2 ribbon of dimensions L = 50 μm, W = 10 μm, and τ = 100 nm. The direction and polarization of the plane wave used to compute the cross section are indicated in the inset. In all cases, the polarization points lie along the x-direction. (b) Same as (a), but for the direction and polarization as indicated in the inset. In all cases, the polarization points lie along the z-direction.

and τ = 100 nm for the directions and polarization indicated in the inset. Notice that the cross section is relatively insensitive to the angle θ, which is remarkable taking into account that θ = 0° corresponds to a plane wave directly impinging on the largest facets (y-direction), while θ = 90° corresponds to a plane wave impinging on the lateral facets (z-direction), which have an area that is 100 times smaller in this example. This obviously means that the absorption efficiency Q_{abs}, defined as the absorption cross section divided by the corresponding geometrical cross section,[39] is around 100 times larger for the lateral facets as compared to the upper and lower ones. Things

https://doi.org/10.1021/acsphotonics.2c01183
ACS Photonics 2022, 9, 3679−3684

are even more striking when one analyzes the role of the ends of the ribbons (the smallest facets). As shown in Figure 3b, the absorption cross section along the x-direction ($\theta = 90°$), that is, along the ends of the ribbon, is comparable to that along the y-direction ($\theta = 0°$), that is, along the direction perpendicular to the upper (or lower) facet (see Figure S3 in the Supporting Information for cross section results for the complementary polarization state). This means that the emission along the ribbon ends has an efficiency that is about 500 times larger than that of the largest facets. Thus, the overall thermal emission of these highly anisotropic nanoribbons is the result of a sizable contribution of all facets. This highly directional emissivity can be understood as follows: First, the emission of the largest facets can be simply explained in terms of the absorption coefficient of a thin film and is a result of the fact that these nanoribbons have a thickness that is smaller than the silica skin depth. On the other hand, the striking emission through the nanoribbons' ends can be explained following the work by Fernández-Hurtado et al.[15] These authors showed that this type of elongated structure made of polar dielectrics behaves as a lossy dielectric waveguide that efficiently absorbs the radiation via the excitation of guided modes along the length of the ribbons. In the Supporting Information, we present a detailed analysis of the nature of the guided modes along the length of the nanoribbons that explains the extraordinary absorptivity/emissivity along the ends of the ribbons. In particular, that analysis shows that the TE modes are much more efficient at emitting and absorbing infrared radiation than the TM ones, which can be ascribed to the much shorter propagation length of the TE modes. This, in turn, explains the pronounced polarization dependence of the cross section along the nanoribbon's ends (compare Figure 3b with Figure S3b).

So far, we have focused on the emission properties of these nanoribbons at room temperature (300 K). Interestingly, Shin et al.[20] found that the total emissivity of these nanoribbons increases monotonically upon decreasing the temperature in the range between 430 and 150 K. In particular, they reported an 8.5-fold enhancement of the total emissivity compared with the thin film case at 150 K for nanoribbons with $L = 400$ μm, $W = 6.28$ μm, and $\tau = 100$ nm. To analyze this issue, we have computed the temperature dependence of the total emissivity. Since it has been experimentally established that the optical properties of SiO_2 do not significantly vary with temperature in the range between 4 and 300 K,[40] we have assumed that the frequency-dependent emissivity does not change with temperature, and the only temperature dependence of $\varepsilon_{\text{Total}}$ comes from the Planck's distribution function, see eq 1. The results for the temperature dependence of the total emissivity for the nanoribbons explored by Shin et al.[20] ($W = 6.28$, 11.5 μm), along with the result for a 100 nm thick film, are shown in Figure 4a. Notice that, contrary to the experimental results, we find that the maximum emissivity is reached at temperatures close to room temperature (300 K), while at lower temperatures the total emissivity clearly diminishes. In fact, the total emissivity for these nanoribbons very much follows the temperature dependence for the thin film case, see Figure 4a. This temperature dependence is actually expected from the fact that, as shown in eq 1, the total emissivity is mainly determined by the convolution between the (temperature-independent) emissivity spectrum and Planck's distribution function $I_{\text{BB}}(\omega,T)$. As shown in Figure 4b, from this convolution, one naturally expects the total emissivity to

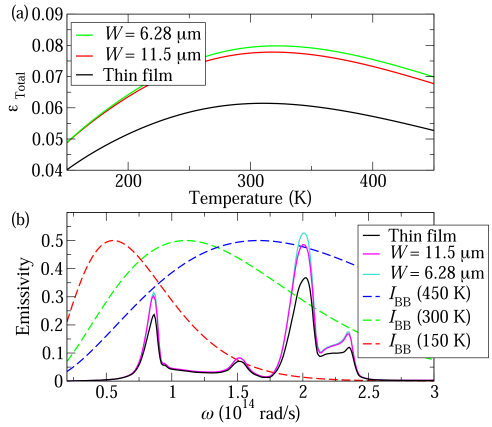

Figure 4. (a) Total emissivity (integrated over frequencies) as a function of temperature for two silica nanoribbons with thickness τ = 100 nm, length L = 50 μm and two different widths, as indicated in the legend. For comparison, we have also included the result for a thin film of thickness τ = 100 nm (black solid line). (b) Emissivity spectra of the three cases considered in (a), solid lines, along with Planck's distribution function I_{BB} (in arbitrary units) at temperatures of 150, 300, and 450 K (dashed lines).

decrease with temperature (as compared to the room temperature case) because the contribution of the high-frequency phonon-polariton resonance progressively diminishes and eventually vanishes. Thus, the experimental findings for the temperature dependence of the total emissivity are certainly puzzling, and it would be highly desirable to conduct further experiments to clarify this issue.

To complete our study, it is interesting to explore the role of the thickness of these ribbons and, in particular, to understand the crossover between the subwavelength regime and the macroscopic one. This crossover is illustrated in Figure 1c for the case of a film of increasing thickness. There we see that as the thickness becomes of the order of the skin depth (~1 μm for a wavelength of 10 μm, i.e., for $\omega \sim 2 \times 10^{14}$ rad/s), there is a crossover from a situation where the thermal emission is volumetric (for thin films) to a situation where the thermal emission becomes a surface phenomenon (for thick films) with much higher total emissivities (reaching $\varepsilon_{\text{Total}} = 0.79$ for the bulk case). We report in Figure 5a the results of a similar study for the thickness dependence of the emissivity spectra of silica

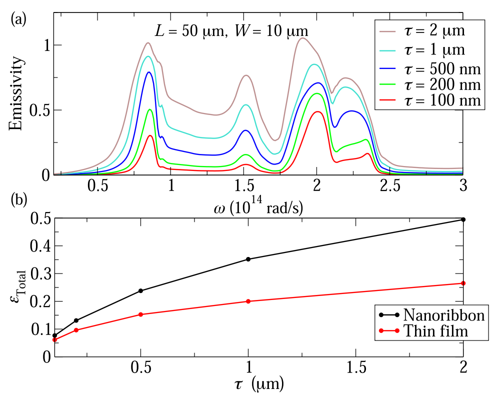

Figure 5. (a) Emissivity spectra for SiO_2 ribbons with L = 50 μm, W = 10 μm, and different values of thickness τ. (b) The total emissivity of the ribbons in (a) and the corresponding thickness dependence for SiO_2 thin films.

https://doi.org/10.1021/acsphotonics.2c01183
ACS Photonics 2022, 9, 3679−3684

ribbons of width $W = 10\ \mu$m ranging from $\tau = 100$ nm to $\tau = 2\ \mu$m, which is the largest system that we were able to simulate with our computational resources. Let us remark that all these examples are still within the subwavelength regime and even the largest thickness is smaller than the skin depth for most frequencies. In spite of these limitations, we can still observe an incipient bulky behavior as the thickness increases. Interestingly, for the 2 μm-thick case, there are some frequencies for which the emissivity is slightly higher than 1, although the total emission is not super-Planckian. In Figure 5b we show the drastic impact that the thickness has on the total emissivity of these ribbons. Notice also that in this regime, the difference between the total emissivities of the ribbons and the corresponding thin films actually increases with thickness. Therefore, overall, these results nicely illustrate the high tunability of the emission properties of these silica ribbons and suggest that the emission properties are much more sensitive to the ribbon's thickness.

■ CONCLUSIONS

In summary, motivated by recent experiments, we have presented a theoretical study of the thermal emission properties of very anisotropic SiO_2 nanoribbons based on numerical simulations within the framework of fluctuational electrodynamics performed with the BEM implemented in the code SCUFF-EM. First of all, we have shown that the thermal emission of these dielectric structures can be largely tuned by playing with their relative dimensions (width and thickness). In particular, we have found that, in agreement with the experimental findings, the total emissivity of subwavelength silica ribbons is clearly enhanced with respect to the thin film case. We have also explained that the thermal properties of these systems are the result of a highly directional emission where all facets contribute decisively, despite their very different geometrical cross sections. Moreover, we have studied the temperature dependence of the emissivity and found that it is maximized at close to room temperature. Overall, our work illustrates that subwavelength objects can emit thermal radiation in a very complex manner that is out of the scope of Planck's law and whose description requires advanced numerical techniques that make use of the rigorous fluctuational electrodynamics theory.

■ ASSOCIATED CONTENT

Supporting Information

The Supporting Information is available free of charge at https://pubs.acs.org/doi/10.1021/acsphotonics.2c01183.

Additional results related to the emissivity of thin films; convergence tests of the BEM used to compute the nanorribons' emissivity; absorption cross section of the nanoribbons; and a discussion on the nature of the guided modes in the nanoribbons to explain their very anisotropic emissivity (PDF)

■ AUTHOR INFORMATION

Corresponding Author

Juan Carlos Cuevas − *Departamento de Física Teórica de la Materia Condensada and Condensed Matter Physics Center (IFIMAC), Universidad Autónoma de Madrid, E-28049 Madrid, Spain;* orcid.org/0000-0001-7421-0682; Email: juancarlos.cuevas@uam.es

Authors

Juan José García-Esteban − *Departamento de Física Teórica de la Materia Condensada and Condensed Matter Physics Center (IFIMAC), Universidad Autónoma de Madrid, E-28049 Madrid, Spain;* orcid.org/0000-0002-4306-3453

Jorge Bravo-Abad − *Departamento de Física Teórica de la Materia Condensada and Condensed Matter Physics Center (IFIMAC), Universidad Autónoma de Madrid, E-28049 Madrid, Spain*

Complete contact information is available at: https://pubs.acs.org/10.1021/acsphotonics.2c01183

Funding

J.J.G.E. was supported by the Spanish Ministry of Science and Innovation through an FPU grant (FPU19/05281). J.B.A. acknowledges financial support from the Ministerio de Ciencia, Innovación y Universidades (RTI2018-098452-B-I00). J.C.C. acknowledges funding from the Spanish Ministry of Science and Innovation (PID2020-114880GB-I00).

Notes

The authors declare no competing financial interest.

■ REFERENCES

(1) Rephaeli, E.; Raman, A.; Fan, S. Ultrabroadband photonic structures to achieve high-performance daytime radiative cooling. *Nano Lett.* **2013**, *13*, 1457−1461.

(2) Raman, A. P.; Anoma, M. A.; Zhu, L.; Rephaeli, E.; Fan, S. Passive radiative cooling below ambient air temperature under direct sunlight. *Nature* **2014**, *515*, 540−544.

(3) Zhai, Y.; Ma, Y.; David, S. N.; Zhao, D.; Lou, R.; Tan, G.; Yang, R.; Yin, X. Scalable-manufactured randomized glass-polymer hybrid metamaterial for daytime radiative cooling. *Science* **2017**, *355*, 1062−1066.

(4) Jaramillo-Fernandez, J.; Whitworth, G. L.; Pariente, J. A.; Blanco, A.; Garcia, P. D.; Lopez, C.; Sotomayor-Torres, C. M. A Self-Assembled 2D Thermofunctional Material for Radiative Cooling. *Small* **2019**, *15*, No. e1905290.

(5) Feng, J.; Santamouris, M.; Gao, K. The radiative cooling efficiency of silica sphere embedded polymethylpentene (TPX) systems. *Sol. Energy Mater.* **2020**, *215*, 110671.

(6) Chen, M.; Pang, D.; Chen, X.; Yan, H. Investigating the effective radiative cooling performance of random dielectric microsphere coatings. *Int. J. Heat Mass Tran.* **2021**, *173*, 121263.

(7) Xiang, B.; Zhang, R.; Luo, Y.; Zhang, S.; Xu, L.; Min, H.; Tang, S.; Meng, X. 3D porous polymer film with designed pore architecture and auto-deposited SiO2 for highly efficient passive radiative cooling. *Nano Energy* **2021**, *81*, 105600.

(8) Yu, Z.; Sergeant, N. P.; Skauli, T.; Zhang, G.; Wang, H.; Fan, S. Enhancing far-field thermal emission with thermal extraction. *Nat. Commun.* **2013**, *4*, 1730.

(9) Tan, Y.; Liu, B.; Shen, S.; Yu, Z. Enhancing radiative energy transfer through thermal extraction. *Nanophotonics* **2016**, *5*, 22−30.

(10) Planck, M.*The Theory of Thermal Radiation*; P. Blakiston Son & Co.: Philadelphia, 1914.

(11) Li, W.; Fan, S. Nanophotonic control of thermal radiation for energy applications. *Opt. Express* **2018**, *26*, 15995.

(12) Cuevas, J. C.; García-Vidal, F. J. Radiative heat transfer. *ACS Photonics* **2018**, *5*, 3896−3915.

(13) Cuevas, J. C. Thermal radiation from subwavelength objects and the violation of Planck's law. *Nat. Commun.* **2019**, *10*, 3342.

(14) Golyk, V. A.; Kruger, M.; Kardar, M. Heat radiation from long cylindrical objects. *Phys. Rev. E: Stat., Nonlinear, Soft Matter Phys.* **2012**, *85*, 046603.

(15) Fernández-Hurtado, V.; Fernández-Domínguez, A. I.; Feist, J.; García-Vidal, F. J.; Cuevas, J. C. Super-Planckian far-field radiative

heat transfer. *Phys. Rev. B: Condens. Matter Mater. Phys.* **2018**, *97*, 045408.
(16) Thompson, D.; Zhu, L.; Mittapally, R.; Sadat, S.; Xing, Z.; McArdle, P.; Qazilbash, M.; Reddy, P.; Meyhofer, E. Hundred-fold enhancement in far-field radiative heat transfer over the blackbody limit. *Nature* **2018**, *561*, 216−221.
(17) Wuttke, C.; Rauschenbeutel, A. Thermalization via Heat Radiation of an Individual Object Thinner than the Thermal Wavelength. *Phys. Rev. Lett.* **2013**, *111*, 024301.
(18) Li, C.; Krachmalnicoff, V.; Bouchon, P.; Jaeck, J.; Bardou, N.; Haïdar, R.; De Wilde, Y. Near-Field and Far-Field Thermal Emission of an Individual Patch Nanoantenna. *Phys. Rev. Lett.* **2018**, *121*, 243901.
(19) Kallel, H.; Doumouro, J.; Krachmalnicoff, V.; De Wilde, Y.; Joulain, K. Thermal emission from a single glass fiber. *J. Quant. Spectrosc. Radiat. Transfer* **2019**, *236*, 106598.
(20) Shin, S.; Elzouka, M.; Prasher, R.; Chen, R. Far-field coherent thermal emission from polaritonic resonance in individual anisotropic nanoribbons. *Nat. Commun.* **2019**, *10*, 1377.
(21) Fenollosa, R.; Ramiro-Manzano, F.; Garín, M.; Alcubilla, R. Thermal Emission of Silicon at Near-Infrared Frequencies Mediated by Mie Resonances. *ACS Photonics* **2019**, *6*, 3174−3179.
(22) Shin, S.; Chen, R. Plasmonically Enhanced Thermal Radiation by Means of Surface Phonon Polaritons. *Phys. Rev. Appl.* **2020**, *14*, 064013.
(23) Abou-Hamdan, L.; Li, C.; Haidar, R.; Krachmalnicoff, V.; Bouchon, P.; De Wilde, Y. Hybrid modes in a single thermally excited asymmetric dimer antenna. *Opt. Lett.* **2021**, *46*, 981−984.
(24) Rytov, S. M.; Kravtsov, Y. A.; Tatarskii, V. I.*Principles of Statistical Radiophysics*; Springer-Verlag: Heidelberg, 1989; Vol. 3
(25) Otey, C. R.; Zhu, L.; Sandhu, S.; Fan, S. Fluctuational electrodynamics calculations of near-field heat transfer in non-planar geometries: A brief overview. *J. Quant. Spectrosc. Radiat. Transfer* **2014**, *132*, 3.
(26) Krüger, M.; Emig, T.; Kardar, M. Nonequilibrium Electromagnetic Fluctuations: Heat Transfer and Interactions. *Phys. Rev. Lett.* **2011**, *106*, 210404.
(27) Rodriguez, A. W.; Ilic, O.; Bermel, P.; Celanovic, I.; Joannopoulos, J. D.; Soljačić, S. G.; Johnson, S. G. Frequency-Selective Near-Field Radiative Heat Transfer between Photonic Crystal Slabs: A Computational Approach for Arbitrary Geometries and Materials. *Phys. Rev. Lett.* **2011**, *107*, 114302.
(28) Rodriguez, A. W.; Reid, M. T. H.; Johnson, S. G. Fluctuating-surface-current formulation of radiative heat transfer for arbitrary geometries. *Phys. Rev. B: Condens. Matter Mater. Phys.* **2012**, *86*, 220302.
(29) Polimeridis, A. G.; Reid, M. T. H.; Jin, W.; Johnson, S. G.; White, K.; Rodriguez, A. W. Fluctuating volume-current formulation of electromagnetic fluctuations in inhomogeneous media: Incandescence and luminescence in arbitrary geometries. *Phys. Rev. B: Condens. Matter Mater. Phys.* **2015**, *92*, 134202.
(30) Edalatpour, S.; Francoeur, M. The Thermal Discrete Dipole Approximation (T-DDA) for near-field radiative heat transfer simulations in three-dimensional arbitrary geometries. *J. Quant. Spectrosc. Radiat. Transfer* **2014**, *133*, 364.
(31) Abraham Ekeroth, R. M.; García-Martín, A.; Cuevas, J. C. Thermal discrete dipole approximation for the description of thermal emission and radiative heat transfer of magneto-optical systems. *Phys. Rev. B: Condens. Matter Mater. Phys.* **2017**, *95*, 235428.
(32) Li, Z.; Li, X.; Liu, H.; Salihoglu, S.; Shen, S. Wiener chaos expansion method for thermal radiation from inhomogeneous structures. *Phys. Rev. B: Condens. Matter Mater. Phys.* **2021**, *104*, 195426.
(33) Rodriguez, A. W.; Reid, M. T. H.; Johnson, S. G. Fluctuating-surface-current formulation of radiative heat transfer: theory and applications. *Phys. Rev. B: Condens. Matter Mater. Phys.* **2013**, *88*, 054305.
(34) Reid, M. T. H.; Johnson, S. G. Efficient computation of power, force and torque in BEM scattering calculations. *IEEE Trans. Antennas Propag.* **2015**, *63*, 3588−3598.
(35) Reid, M. T. H.SCUFF-EM. https://github.com/homerreid/scuff-EM (accessed Feb 16, 2021).
(36) Modest, M. F.*Radiative Heat Transfer*, 3rd ed.; Academic Press: New York, 2013.
(37) Palik, E. D.*Handbook of Optical Constants of Solids*; Academic Press: London, 1985.
(38) Caballero, B.; García-Martín, A.; Cuevas, J. C. Generalized scattering-matrix approach for magneto-optics in periodically patterned multilayer systems. *Phys. Rev. B: Condens. Matter Mater. Phys.* **2012**, *85*, 245103.
(39) Bohren, C. F.; Huffman, D. R.*Absorption and Scattering of Light by Small Particles*; Wiley: New York, 1998.
(40) Ordonez-Miranda, J.; Joulain, K.; De Sousa Meneses, D.; Ezzahri, Y.; Drevillon, J. Photonic thermal diode based on superconductors. *J. Appl. Phys.* **2017**, *122*, 093105.

https://doi.org/10.1021/acsphotonics.2c01183
ACS Photonics 2022, 9, 3679−3684